

Competition between Langmuir and Upper-Hybrid Turbulence in a High-Frequency-Pumped Ionosphere

B. Thidé,^{1,*} E. N. Sergeev,² S. M. Grach,^{2,†} T. B. Leyser,¹ and T. D. Carozzi³

¹Swedish Institute of Space Physics, P.O. Box 537, SE-751 21 Uppsala, Sweden

²Radiophysical Research Institute, B. Pecherskaya 25, Nizhniy Novgorod, RU-603 950, Russia

³Space Science Centre, University of Sussex, Brighton, BN1 9QT, United Kingdom

(Received 7 April 2005; published 15 December 2005)

We show how the secondary escaping radiation, also known as stimulated electromagnetic emission (SEE), from the ionosphere irradiated by a high-intensity radio beam, can be used to study both reflection altitude ponderomotive parametric instabilities and upper-hybrid altitude thermal parametric instabilities. This has allowed us to observe the transfer of energy from smaller to higher sideband frequency offsets and to identify a new transient SEE feature.

DOI: [10.1103/PhysRevLett.95.255002](https://doi.org/10.1103/PhysRevLett.95.255002)

PACS numbers: 52.35.Mw, 52.35.Ra, 52.25.Os, 94.20.Tt

It was discovered experimentally already in 1981 that when a narrow-band high-frequency (hf) radio beam of high intensity irradiates the ionosphere at a frequency f_0 which is close to the local ionospheric plasma frequency f_p , a structured, wide-band secondary radiation escapes from the interaction region [1], a phenomenon now known as stimulated electromagnetic emission (SEE) [2–21]. By varying the injected hf beam systematically in terms of frequency, intensity, and duty cycle and analyzing the secondary radiation, and hence the associated hf radio beam-excited ionospheric plasma turbulence and wave conversion processes, we have been able to study the competition between the effects due to ponderomotive parametric instabilities (PPI) [22–24] and those due to thermal parametric instabilities (TPI) [25,26].

The dynamics of the secondary radiation has been studied earlier [2,4,8,10,11,16–18,21]. However, due to instrumental shortcomings, these studies often had resolution limitations in time Δt or in frequency $\Delta \nu$. The use of an HP3587S 23 bit baseband signal analysis system with a maximum sampling rate of 20 Msamples/s allowed us to perform the measurements reported here, carried out at the purpose-built space radio research facility Sura near Nizhniy Novgorod, Russia (geographical coordinates 56.13°N, 46.10°E), with sufficient resolution, limited only by the fundamental relation $\Delta t \Delta \nu \approx 1$.

The general physical scenario is as follows: during the first few milliseconds after the arrival of the leading edge of a strong hf radio beam injected into the unperturbed overhead ionosphere, the PPI develop in a region a few hundred meters below the hf reflection point z_0 at which $f_p(z_0) = f_0$, typically in the 3–10 MHz range. Since at z_0 the hf pump field \mathbf{E}_0 is parallel to the geomagnetic field, Langmuir modes in this region are launched predominantly along this direction. During the period 0.5–10 s, the TPI develop typically some 2–5 km below z_0 , near the upper-hybrid (UH) altitude z_{UH} , at which $f_p(z_{UH}) = [f_0^2 - f_{ce}^2(z_{UH})]^{1/2}$ and f_{ce} is the local ionospheric electron cyclotron frequency. Here \mathbf{E}_0 has a considerable component

perpendicular to the geomagnetic field and excites upper-hybrid waves propagating mainly across the magnetic field, and therefore also across the small-scale geomagnetic field-aligned irregularities of plasma density (striations) which are concurrently being formed through the action of TPI near z_{UH} . Since different plasma mode interactions produce distinctive features in the secondary radiation, the SEE method allows systematic stimulus-response studies of ionospheric turbulence without the need of additional probing radio waves, scatter radars, or *in situ* spacecraft probes.

A secondary radiation component known to be directly related to the PPI excitation near z_0 is the redshifted ponderomotive narrow continuum feature NC_p [18,21]. The TPI associated radiation generated near z_{UH} has a much richer, yet systematic and reproducible spectral structure [3–11,13,14,16–20]. Several distinctive spectral features such as the down-shifted, up-shifted, and broad up-shifted maxima (DM, UM, and BUM, respectively), and the narrow thermal and broad continua (NC_{th} and BC, respectively), have been identified in the secondary radiation. These features are linked to specific plasma processes and exhibit a dramatic dependence on the relation between f_0 and electron cyclotron harmonics $sf_{ce}(z_{UH})$, $s = 3, 4, 5, 6, 7$ [see Refs. [3,5,9,14,16–18,20]]. In particular, a coincidence of f_0 with sf_{ce} is identified by the suppression of the down-shifted maximum (DM) spectral feature, generated by the nonlinear interaction between hf-excited upper-hybrid modes, lower hybrid modes, and striations [5,6,8].

The excitation of striations and concomitant anomalous absorption (AA) near z_{UH} , caused by a scattering of the hf pump wave (PW) off the striations into UH waves [25] are suppressed for $f_0 = sf_{ce}(z_{UH})$ [9,27]. This allowed us to step f_0 in a systematic manner from $5f_{ce}(z_{UH}) - 30$ kHz to $5f_{ce}(z_{UH}) + 80$ kHz, where $f_{ce}(z_{UH})$ varied naturally between 1.329 MHz and 1.356 MHz, to suppress or enhance the UH-associated secondary radiation. Likewise, selecting an interpulse period (IPP) of 2 s while varying

the pulse length from 300 μ s to 500 ms, it was possible to excite ionospheric turbulence under conditions from “cold start” to “preconditioned” thus having control over the level of TPI and, consequently, striations and AA. In addition, this experimental technique allowed us to integrate over subsequent pulses for improved statistics and enhancement of systematic features. The effective radiated pump power P (transmitter output power \times 23 dB antenna gain) in the experiments ranged from 80 to 180 MW thus producing an initial $|\mathbf{E}_0(z_0)|$ ranging from 3–5 V/m to 4.5–6 V/m, well above the 0.2–0.3 V/m parametric instability threshold even if linear absorption is accounted for.

In Fig. 1, the average of two data sets on the temporal evolution of the SEE spectra and the intensity of the reflected PW at $f_0 = 6778$ kHz $\approx 5f_{ce}(z_{UH})$ are displayed. The two sets consist of 12 consecutive runs, the first with 20 ms hf pulses and the second with 200 ms pulses. For $f_0 \approx sf_{ce}$ and IPP = 2 s, such short pulses do not give rise to any significant striation formation, AA, or any other UH-related phenomena. Hence, Fig. 1 represents PPI radiation phenomena near z_0 . The initial periodic intensity peaks are due to multiple sky-ground hops of the leading edge of the PW pulse; the spectral lines seen at $\Delta f = f - f_0 \approx 20$ kHz and ± 30 kHz are caused by radio station interference and hf pump transmitter effects. For $t \sim 1.3$ –1.5 ms the NC_p feature grows while the reflected PW decreases up to 20 dB. For $t \sim 1.5$ –2.0 ms the NC_p has maximum intensity for about $\Delta f = -10$ kHz to 0 kHz. As t increases, the radiation intensity near f_0 diminishes simultaneously with a growth further out in the lower sideband. For $t \approx 5$ ms the spectrum width attains a

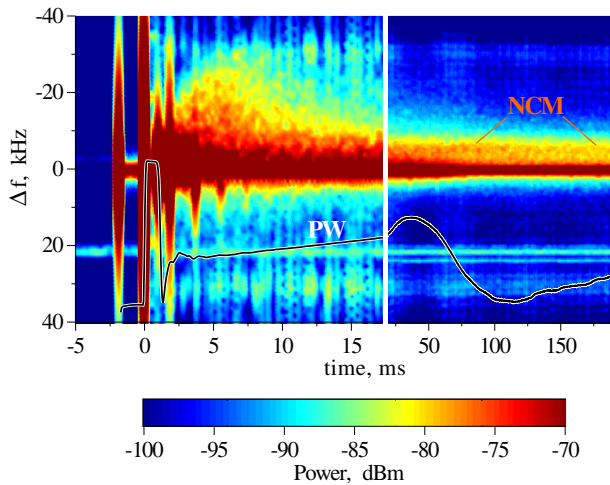


FIG. 1 (color online). SEE spectra (–5)–20 ms (left) and 20–200 ms (right) after hf pump turn-on. The early period spectral resolution is $\Delta\nu = 1$ kHz with 50 μ s between subsequent spectra. For the late period $\Delta\nu = 0.5$ kHz with 500 μ s between spectra. The line labeled PW depicts the temporal evolution of the reflected pump wave. September 26, 1998, 14:52–15:26 LT; $f_0 = 6778$ kHz $\approx 5f_{ce}$; $P \approx 180$ MW.

maximum value of about 30 kHz. Later, the SEE intensity decreases for all frequencies in correlation with a 10 dB increase of PW intensity until $t = t_s \approx 50$ ms. Following this, the PW intensity decreases and exhibits damped quasi-periodical oscillations or “spikes” [4], while the NC_p intensity continues to decrease. At this time, a weak spectral maximum at -6 kHz $< \Delta f < -4$ kHz appears in the background of the decreasing NC_p . This is seen in the right-hand part of Fig. 1 for $t > 50$ ms. We call this feature NCM, the narrow continuum maximum.

The NCM spectral feature was observed for f_0 in a range ± 30 kHz around $5f_{ce}$, and its initial temporal behavior was similar to that for $f_0 \approx 5f_{ce}$. This is illustrated in Fig. 2 which shows an example of the temporal evolution of the SEE spectra for a cold start with $P = 80$ MW at $f_0 \approx 5f_{ce}$ (left-hand panel) and at $f_0 \approx 5f_{ce} - 10$ kHz (right-hand panel). For both pump frequencies the behavior until $t \sim 3$ –4 s is similar to the one described above for $P = 180$ MW, but with a longer time scale. For $t \approx 4.5$ –5 s and $f_0 < 5f_{ce}$ the DM feature appears and its intensity equals that of the NCM; later, after a noticeable growth of the UH-associated DM and BC spectral features, the NCM is not distinguished in the SEE spectrum. For $f_0 \approx 5f_{ce}$ the DM and BC do not exist, and the NCM remains in the spectrum until the stationary stage, although a decrease of the NCM intensity with t is correlated with a growth of the UH-associated UM and BUM features.

Figure 3 displays a set of stationary SEE spectra for different gyroharmonic frequency mismatches $\delta f = f_0 - 5f_{ce}$. The NCM is seen only in the spectrum denoted $\delta f \sim 0$ kHz which also exhibits the weakest DM. In the spectrum denoted $\delta f \sim 0$ kHz (AA) with the same DM intensity, the NCM can hardly be distinguished. The latter spectrum was obtained for a rather well-developed anomalous absorption. A reanalysis of earlier experimental data

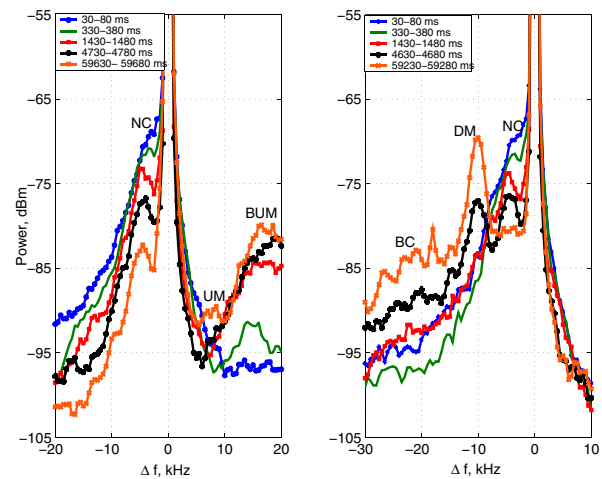


FIG. 2 (color online). Temporal evolution of secondary radiation (SEE) spectra after PW turn-on for $f_0 = 6645$ kHz $\approx 5f_{ce}$ (left panel) and $f_0 = 6635$ kHz $\approx 5f_{ce} - 10$ kHz (right panel). September 24, 1998, 17:22–17:26 LT; $\Delta\nu = 0.5$ kHz; $P \approx 80$ MW.

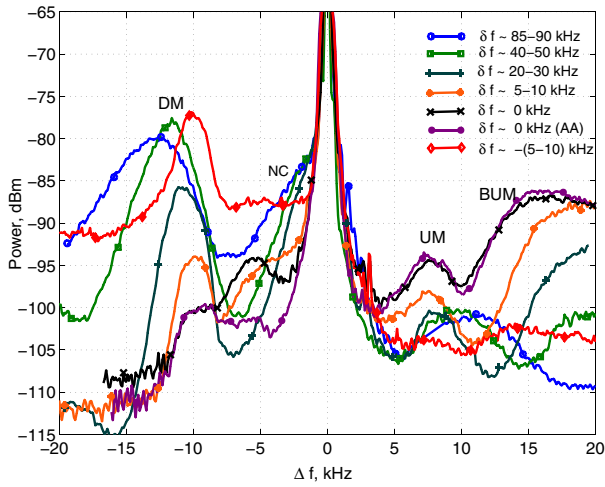


FIG. 3 (color online). Stationary SEE spectra for different gyroharmonic frequency mismatches $\delta f = f_0 - 5f_{ce}$. September 23–24, 1998, 14:50–17:20 LT; $\Delta\nu = 100$ Hz; $P \approx 80$ MW.

shows that the NCM can be sporadically distinguished in stationary spectra also for $f_0 \approx 4f_{ce}$ and $f_0 \approx 6f_{ce}$. When f_0 is not close to a gyroharmonic, the NCM is seen in the radiation spectra before the development of the BC and DM takes over. Notice that the NCM frequency shift $\Delta f_{NCM} = f_0 - f_{NCM}$ increases with pump power P and time t ; see the left-hand panel of Fig. 2.

For a preconditioned ionosphere, when striations and AA do not disappear completely between successive hf pump pulses, the UH-related features develop much faster after a pump turn-on than for a cold start. In this case neither NC_p nor NCM are observed. For $\Delta f_{DM} < \Delta f < 0$ SEE develops concurrently with the DM. Furthermore, for $f_0 > 5f_{ce}$ the slopes of the stationary SEE spectrum in this frequency range and at the lower frequency flank of the DM are very close and narrow down as f_0 approaches $5f_{ce}$. This is seen in Fig. 3 for $\delta f \geq 20$ kHz and for $\delta f \sim 0$ kHz (AA). This shows that for a preconditioned ionosphere the secondary radiation in the NC frequency range is closely related to the presence of striations and is generated in the UH region due to a TPI process. Therefore, we denote it NC_{th} (“thermal” in contrast to “ponderomotive”). For small mismatches $\delta f \sim 5$ –10 kHz, as well as for $\delta f = 0$ kHz, the UH turbulence is suppressed, and the NC_p (NCM) radiation dominates over the NC_{th} . In fact, in the mismatch range $-10 \text{ kHz} \leq \delta f \leq -5 \text{ kHz}$, the SEE in the NC frequency range behaves like a part of the BC feature; see Figs. 2 and 3. Most probably, this is due to the involvement of electron Bernstein modes in the SEE generation [28,29], which again is related to TPI. Notice that a slow joint NC and DM development was observed previously only for f_0 far from sf_{ce} and near the PPI threshold [13]; the narrowing of the NC_{th} when f_0 approaches sf_{ce} was pointed out in Ref. [13] and has been observed earlier for $f_0 \approx 4f_{ce}$ [20].

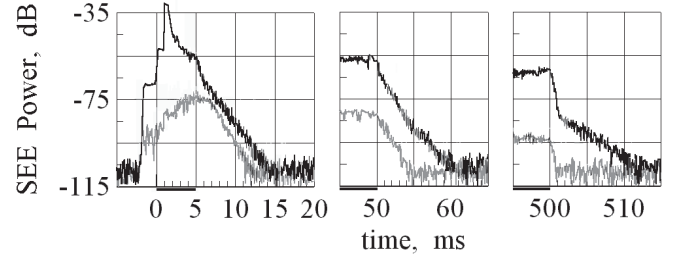


FIG. 4. SEE decay after PW turn-off for $\Delta f \approx -8$ kHz ($\Delta\nu = 4$ kHz, black lines) and $\Delta f \approx -30$ kHz ($\Delta\nu = 2.5$ kHz, gray lines) for PW pulse lengths $\tau = 5, 50,$ and 500 ms. For clarity, sharp periodic peaks caused by multiple reflections of the trailing edges of the PW pulses have been removed. The times and dates are the same as for Fig. 1.

Figure 4 shows the decay of the intensity of SEE in the NC frequency range after pump turn-offs for different hf pump pulse lengths τ , corresponding to different stages of the SEE development, for $\Delta f = -8$ kHz and -30 kHz; effects related to the trailing edge of the PW pulse prevented a measurement of the SEE decay for smaller $|\Delta f|$. For short-duration pumping ($\tau = 5$ or 10 ms), when the NC_p is strongest and widest, the decay of the NC_p at $\Delta f = -8$ kHz appears immediately after the PW turn-off, while at the low-frequency flank of the spectrum the decay appears after a time delay of about 1.5–2 ms. The SEE e -folding decay time of about 0.8–1.0 ms, which is the same for all Δf , is much shorter than the collisional damping time of Langmuir waves $\nu_e^{-1} \approx 2.5$ ms. This difference between the observed decay time and the expected collisional damping time is most likely related to collisionless damping of Langmuir waves on suprathermal electrons (photoelectrons) in the ionosphere. For pulse lengths $\tau \geq 50$ ms the delay disappears and the NC_p decay is a two-step process. For $\tau = 500$ ms the first step e -folding decay time is 0.20–0.26 ms but in the second step it is much longer and close to the collisional damping time. A presence of a second collisional step in the SEE relaxation is typical for Langmuir and UH turbulence of weak intensity [17].

The experiments show that the temporal evolution of the secondary radiation proceeds in three stages: an initial, an intermediate, and an UH-related stage. During the initial and intermediate stages the SEE features (NC_p and NCM) do not depend on the mismatch between f_0 and $5f_{ce}$. This means that these features are associated with Langmuir waves propagating mainly along the geomagnetic field near z_0 . During the first few milliseconds of hf pumping (initial stage) the NC_p is the only feature in the SEE spectrum. The flattening and widening of the NC_p , as well as the delay of the start of the decay, indicate a Langmuir turbulence energy transfer in the spectrum towards lower frequencies. Such a transfer is typical for weak turbulence regimes of PPI [10,16,23], also known as the parametric decay instability (PDI), and was previ-

ously observed only for the relaxation of the SEE BC feature [10,14]. Because of the swelling of the electric field of the pump wave in the region immediately below z_0 [30], the PDI develops rapidly in this region. The rather wide NC_p spectrum of approximately 30 kHz during this stage shows that the radiation must be generated a few hundred meters below z_0 . Otherwise the secondary radiation would not escape from the ionosphere. On the other hand, near z_0 strong turbulence is expected to occur [24]. We did not find any clear evidence of SEE at $\Delta f > 0$, corresponding to so-called “free mode” of Langmuir waves [31,32]. SEE with a spectral shape as described in [12] were observed only when pump pulse edges happened to leak into our Fourier analysis time window.

During the intermediate stage, concurrent with an NC_p decrease and PW spikes, the NCM appears in the spectra against the NC_p background. We interpret this NCM appearance as a further downward displacement of the Langmuir related SEE source. The increase in Δf_{NCM} with t and P is an additional evidence for such a displacement. In particular, the predicted PDI maximum in the Langmuir wave spectrum should appear at $\Delta f \approx -f_0(m_e/m_i)^{1/2} \times (\Delta z/H)^{1/2}$, where m_e/m_i is the electron-to-ion mass ratio, H the ionospheric scale height, and Δz the distance from the hf reflection point [22]. If we attribute NCM to the PDI, the $|\Delta f_{NCM}|$ increase would be related to a growth in Δz . The latter is conditioned by a downward expansion, with P or t , of the region in which the PDI develops. Such an interpretation requires, however, further theoretical studies of the spatiotemporal behavior of the PPI in the ionosphere. A downward motion of the pump-driven Langmuir turbulence with a formation of a spectral maximum was observed with the Arecibo incoherent scatter radar [32,33]. For P small but still exceeding the PDI threshold, the NC_p and NCM survive longer in the SEE spectrum because of the longer time needed for AA to develop.

For long-duration pumping at $f_0 \neq sf_{ce}$, a further decrease in the NC_p intensity occurs concurrently with a growth of the DM, NC_{th} , and other features related to the excitation of UH waves and striations during the TPI processes (third stage). For a preconditioned ionosphere, the NC_p does not show up at all in the SEE spectra. This is due to energy losses of the PW and the secondary radiation on UH modes caused by AA or, in other words, by a strong shielding of the NC_p generation region due to striations. For $f_0 \approx sf_{ce}$, the UH turbulence is suppressed or totally quenched, which means that NC_p dominates in the SEE spectra even during the stationary stage. The position of the NCM in the stationary SEE spectrum is close to that of the down-shifted peak (DP) feature, [3,9,18], but the identity of the DP and NCM requires further proof.

We acknowledge the financial support from the Swedish Research Council, the Swedish Royal Academy of Sciences, INTAS (Grant No. 03-51-5583), and the

Russian Foundation for Basic Research (Grants No. 04-02-17544 and No. 03-02-16309).

*Also at LOIS Space Centre, Växjö University, SE-351 95 Växjö, Sweden.

Electronic address: bt@irfu.se

†Also at Radiophysical Faculty, Nizhniy Novgorod State University, Nizhniy Novgorod, Russia.

- [1] B. Thidé, H. Kopka, and P. Stubbe, *Phys. Rev. Lett.* **49**, 1561 (1982).
- [2] B. Thidé *et al.*, *Radio Sci.* **18**, 851 (1983).
- [3] P. Stubbe *et al.*, *J. Geophys. Res.* **89**, 7523 (1984).
- [4] G.N. Boiko *et al.*, *Radiophys. Quantum Electron.* **28**, 259 (1985).
- [5] T.B. Leyser *et al.*, *Phys. Rev. Lett.* **63**, 1145 (1989).
- [6] T.B. Leyser *et al.*, *Phys. Rev. Lett.* **68**, 3299 (1992).
- [7] T.B. Leyser *et al.*, *J. Geophys. Res.* **98**, 17 597 (1993).
- [8] T.B. Leyser *et al.*, *J. Geophys. Res.* **99**, 19 555 (1994).
- [9] P. Stubbe *et al.*, *J. Geophys. Res.* **99**, 6233 (1994).
- [10] E.N. Sergeev *et al.*, *Adv. Space Res.* **15**, No. 12, 63 (1995).
- [11] B. Thidé *et al.*, *J. Geophys. Res.* **100**, 23 887 (1995).
- [12] P. Y. Cheung *et al.*, *Phys. Rev. Lett.* **79**, 1273 (1997).
- [13] V.L. Frolov *et al.*, *Radiophys. Quantum Electron.* **40**, 731 (1997).
- [14] E.N. Sergeev *et al.*, *J. Atmos. Sol. Terr. Phys.* **59**, 2383 (1997).
- [15] P. Y. Cheung *et al.*, *Phys. Rev. Lett.* **80**, 4891 (1998).
- [16] S.M. Grach *et al.*, *J. Atmos. Sol. Terr. Phys.* **60**, 1233 (1998).
- [17] E.N. Sergeev *et al.*, *Radiophys. Quantum Electron.* **41**, 206 (1998).
- [18] T.B. Leyser, *Space Sci. Rev.* **98**, 223 (2001).
- [19] V.L. Frolov *et al.*, *Geophys. Res. Lett.* **28**, 3103 (2001).
- [20] T. Carozzi *et al.*, *J. Geophys. Res.* **106**, 21 395 (2001).
- [21] V.L. Frolov *et al.*, *J. Geophys. Res.* **109**, A07304 (2004).
- [22] F.W. Perkins, C.R. Oberman, and E.J. Valeo, *J. Geophys. Res.* **79**, 1478 (1974).
- [23] Y.I. Al’ber *et al.*, *Sov. Phys. JETP* **39**, 275 (1974).
- [24] D.F. DuBois, A.H. Rose, and D. Russel, *J. Geophys. Res.* **95**, 21 221 (1990).
- [25] S.M. Grach *et al.*, *Radiophys. Quantum Electron.* **20**, 1254 (1977).
- [26] V.V. Vas’kov and A.V. Gurevich, *Sov. Phys. JETP* **46**, 487 (1977).
- [27] P.V. Ponomarenko, T.B. Leyser, and B. Thidé, *J. Geophys. Res.* **104**, 10 081 (1999).
- [28] S.M. Grach and M.M. Shvarts, in *Vth Suzdal URSI Symposium on the Modification of Ionosphere ISSMI’98, Book of Abstracts* (Russian Academy of Sciences, Suzdal, Russia, 1998), p. 39.
- [29] V.V. Vas’kov and N.A. Ryabova, *Radiophys. Quantum Electron.* **45**, 440 (2002).
- [30] B. Thidé and B. Lundborg, *Phys. Scr.* **33**, 475 (1986).
- [31] P. Y. Cheung *et al.*, *J. Geophys. Res.* **97**, 10 575 (1992).
- [32] D.F. DuBois *et al.*, *Phys. Plasmas* **8**, 791 (2001).
- [33] J.A. Fejer, M.P. Sulzer, and F.T. Djuth, *J. Geophys. Res.* **96**, 15 985 (1991).